Switched Reluctance Machine Drives for Electrical Vehicle Propulsion – Optimal Control with Regard to the Losses in Machine and Converter

Wei Peng[1] Korawich Niyomsatian[2] Jeroen Van den Keybus[2] Adrian-Cornel Pop[3] Johan Gyselinck[1]

[1]Université Libre de Bruxelles
BEAMS Dpt
50, Av. F. Roosevelt, B-1050 Brussels, Belgium
Email: johan.gyselinck@ulb.ac.be
wei.peng@ulb.ac.be

[2]Triphase NV
Romeinse straat 18,
3001 Heverlee, Belgium
Email:
jeroen.vandenkeybus@triphase.com
korawich.niyomsatian@triphase.com

[3]Brose Fahrzeugteile GmbH & Co. Kommanditgesellschaft,
Ohmstraße 2a
D-97076 Würzburg, Germany
Email: adriancornel.pop@brose.com

***Abstract*—This paper deals with the losses of Switched Reluctance Machine Drives (SRDs) for electric vehicle propulsion, consisting of the losses in the Switched Reluctance Machine (SRM) and the converter, across some operating regions based on different control strategies, namely Firing Angle (FA) control and Torque Sharing Function (TSF) control. The SRM model which takes into account copper losses and converter losses is obtained through MATLAB/Simulink. The losses and efficiencies in the machine, the converter and the SRD as function of speed and average torque are compared for a 30 kW peak 8/6 SRD.**

Keywords*—*switched reluctance machine (SRM); switched reluctance machine drive (SRD); copper losses; torque sharing function.

I. INTRODUCTION

There are considerable demands for developing electrical motors with high torque density, high efficiency and low cost for the propulsion of electrical vehicles (EVs) [1]. The Switched Reluctance Machine (SRM) is one of the competitive candidates for EVs, besides permanent magnet synchronous machines and induction machines, thanks to some significant advantages, such as simple structure, low cost and rotor robustness. Nevertheless, considerable efforts are still under way to further reduce losses and output torque ripple of Switched Reluctance Machine Drives (SRDs), which are along with Noise Vibration and Harshness (NVH) the main drawback of these drives.

The Firing Angle (FA) control is the basic approach for controlling average torque at a given speed. The three main parameters of this control are the turn-on angle, the turn-off angle and the reference current [19]. The hysteresis bandwidth for the chopping around the reference current is a secondary parameter. The optimization of the control consists of finding the optimum value of the three parameters for each average torque and speed combination, i.e. such that e.g. the torque ripple is minimized, the losses are minimized, or a combination of both.

A more effective method to minimize torque ripple and losses in SRMs at low speed is TSF control and current profiling control [2-10]. The instantaneous torque of the individual phases is defined through suitable TSFs, i.e. their relative contribution to the total torque as function of rotor position. During the phase commutation intervals of an 8/6 SRM, 2 phases (out of 3, 4 or more) contribute to the instantaneous torque. The share of the incoming phase increases (from 0 up to 100%), while the share of the outgoing phase decreases (from 100% down to 0%).

Five different kinds of TSFs are proposed in literature: linear [4], exponential [5], sinusoidal [6], cubic [7] and piecewise cubic TSF [8]. The name indicates the type of variation of the TSFs (as function of the rotor position) during the commutation intervals.

Piecewise cubic TSFs provide the lowest copper losses as well as an extension of the torque-speed region in which smooth torque can be produced (ignoring torque ripple due

978-1-4673-6785-1/15/$31.00 É 2015 European Union

to chopping), other TSFs all have the same minimum copper losses approximately [8-9].

The losses of SRDs mainly depend on operating conditions, control strategies, topologies of the power converter, and characteristics of the power semiconductor devices. To reduce the losses of the SRDs in EVs applications, the attention should be paid on the control strategies for the following reasons: 1) The operating conditions (driving cycles) of EVs can vary in dependence on different drivers and applications. 2) The characteristics of the semiconductor devices depend on the rating of the devices chosen to build converters, which is application-specific. 3) The topologies of the power converter installed in EVs are probably subjected to the most reliable ones. This paper makes the comparison of the losses in the SRDs (losses in the machine and in the converter) between being controlled by FA control and TSF control strategies.

In this paper, we consider the very common SRD converter which comprises an asymmetrical H-bridge converter per phase of the machine. It is capable of feeding each phase independently and even of running the machine under faulty conditions due to the isolation of a phase fault [14]. Generally, it is difficult to obtain the analytical results of the converter losses for SRDs due to its nonlinear characteristics. Still, the direct numerical calculation is time consuming. To avoid this problem, the converter losses were approximately estimated without circuit simulation in the past researches. In other words, they overlooked the dynamic behaviors of the system (i.e. the varying output currents due to varying inductance of the machine according to the rotor positions) and considered the losses only at one particular operating condition [11-13]. Moreover, the switching frequency is assumed constant in [13]. This can lead to inaccurate data for EVs applications, especially when FA control is used. In this paper, the converter losses are estimated online based on the look-up tables of semiconductor parameters constructed from the manufacturer datasheet.

This paper is structured in seven sections. In Section II, a Finite Element (FE) based on electromagnetic model is obtained for the magnetic characterization of the SRM. Sections III and IV deal with FA control and piecewise cubic TSF control strategies of the SRMs respectively. Section V describes the power electronics model of the asymmetric H-bridge converter to evaluate the different control strategies in terms of semiconductor losses in the power converter. The simulation results are presented in Section VI considering different load (average torque and speed) conditions. Copper losses in the SRM for these two control strategies as function of speed and average torque are obtained. The comparisons of different control strategies based on the losses and efficiencies in the machine, the converter and the SRD are obtained in this section. Finally, conclusions are drawn in the last section.

II. Finite Element Analysis Using Gmsh and GetDP

Finite element models allow for accurate magnetic analysis of SRMs (and other types of electrical machines). The two following open-source programs are chosen for this work: Gmsh [15] and GetDP [16].

Gmsh can be used for making and meshing geometrical 2D and 3D models, whereas GetDP is used for the FE computation (magnetic, elastic or coupled, 2D or 3D, static, frequency domain or time stepping). These two programs can be run together from a user-friendly GUI (inside Gmsh), named Open Numerical Engineering LABoratory, ONELAB [17]). Some complete examples of electric machine models (magnetics only), including an SRM model, are publicly accessible [18].

Figure 1 shows the SRM modelling interface developed in ONELAB/Gmsh/GetDP. In this paper, a 15 kW 8/6 SRM is considered. The geometrical dimensions of the studied machine are gathered in Table I. Flux linkage curves for the mentioned model are given in figure 2. Its rated values are 15 kW, 90 Nm at a base speed of 1500 rpm and its peak values are approximately 30 kW, 10 krpm and 200 A.

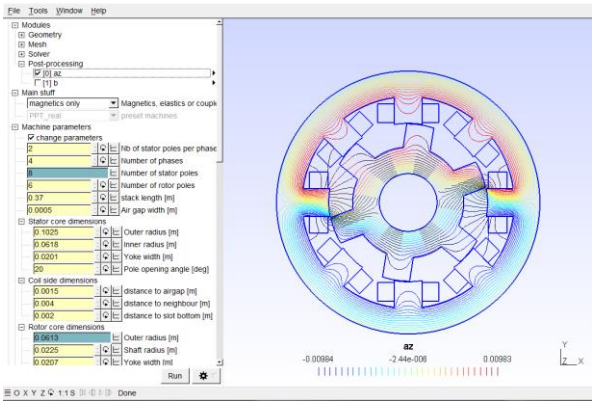

Fig. 1: SRM modelling interface developed in ONELAB/Gmsh/ GetDP for magneto-elastic FE analysis, with part of the menu shown on the left and flux lines in the 8/6 machine shown on the right

TABLE I: GEOMETRICAL DIMENSIONS OF THE SRM

Parameter	***Symbol***	***Value***
Number of phases	N_{ph}	4
Stator outer diameter	D_{out}	205 mm
Rotor outer diameter	D_r	122.6 mm
Stator pole arc	β_s	20°
Rotor pole arc	β_r	20°
Airgap width	g	0.5 mm
Stack length	L_{stk}	185 mm
Number of turns per coils (2 coils in a phase connected in parallel)	N	50

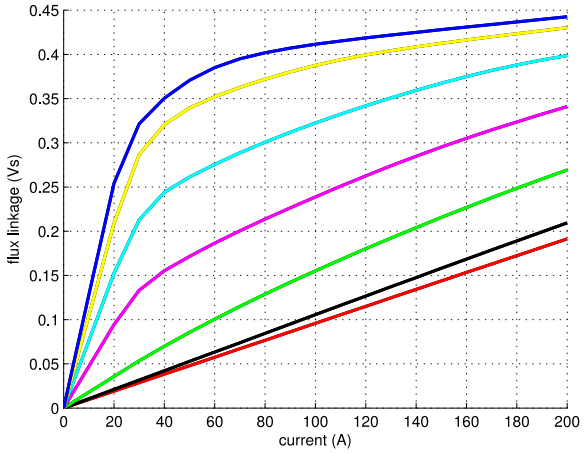

Fig. 2: Flux-linkage curves of the 8/6 SRM (7 curves from aligned position, 0°, till completely misaligned position, 30°, in steps of 5°)

III. Firing Angle Control Strategy

At lower speeds the torque is limited only by the current, which is regulated either by voltage PWM or current regulation. As the speed increases, the back-EMF increases to a certain level, and if there is insufficient voltage available to regulate the current, then the firing angles are controlled to produce the desired torque. Many applications require a combination of a high-speed and a low-speed control mode [19].

Figure 3 shows the torque control block diagram with firing angle control method for a four-phase SRM. It is based on look-up tables of the reference current i^*, turn-on angle θ_{on} and turn-off angle θ_{off} as function of reference electromagnetic torque T^* and speed N. The MATLAB function fminsearchbnd has been used in this paper, and the average torque has been maximized for the FA control.

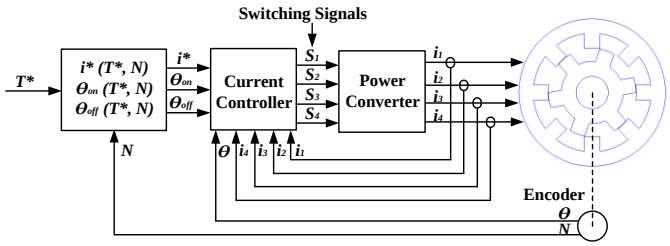

Fig. 3: Torque control block diagram with FA control for a 4-phase SRM

IV. Torque Sharing Function Control Strategy

The origin of the torque ripple of SRMs is twofold: the commutation between two phases on the one hand, and the hysteresis control of the phase currents on the other hand. TSF is an effective approach to implement the control in which reference torques for individual phases are defined assuming the total torque stays at a constant level in SRMs, so the first origin of the torque ripple can be eliminated theoretically. In the commutation region of the ascending and descending profiles of the torque waveforms, both phases contribute to the output torque production. Figure 4 shows the torque control block diagram with TSF control method. The input torque reference value T^* is split up into individual torque references for each phase through the TSF block as function of rotor position. The four torque references T_1^*, T_2^*, T_3^* and T_4^* are converted into current reference signals i_1^*, i_2^*, i_3^* and i_4^* by the Torque-to-Current block. The reference currents are affected through the hysteresis current controller.

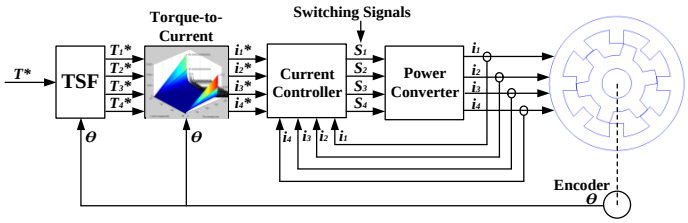

Fig. 4: Torque control block diagram with TSF control for a 4-phase SRM

A. Conventional TSFs

There are four conventional TSFs which can be classified as linear, sinusoidal, exponential and cubic [4-8]. Figure 5 shows the typical profiles of these TSFs. The reference phase torque T_k^* is obtained by different sharing reference curves for constant torque production.

It can be defined as follows:

$$T_k^*(\theta) = \begin{cases} 0, & 0 \le \theta \le \theta_{on} \\ T^* \cdot f_{rise}(\theta), & \theta_{on} < \theta < \theta_{on} + \theta_{ov} \\ T^*, & \theta_{on} + \theta_{ov} \le \theta \le \theta_{off} - \theta_{ov} \\ T^* \cdot f_{fall}(\theta), & \theta_{off} - \theta_{ov} < \theta < \theta_{off} \\ 0, & \theta_{off} \le \theta \le \theta_p \end{cases} \quad (1)$$

where θ_{on} and θ_{off} represent the turn-on and turn-off angles, θ_p the rotor period and θ_{ov} the overlap angle. Functions f_{rise} and f_{fall} represent the rising and falling phase torques of the torque sharing functions which is used during phase commutation. Function f_{rise} rises from 0 to 1, and function f_{fall} falls from 1 to 0.

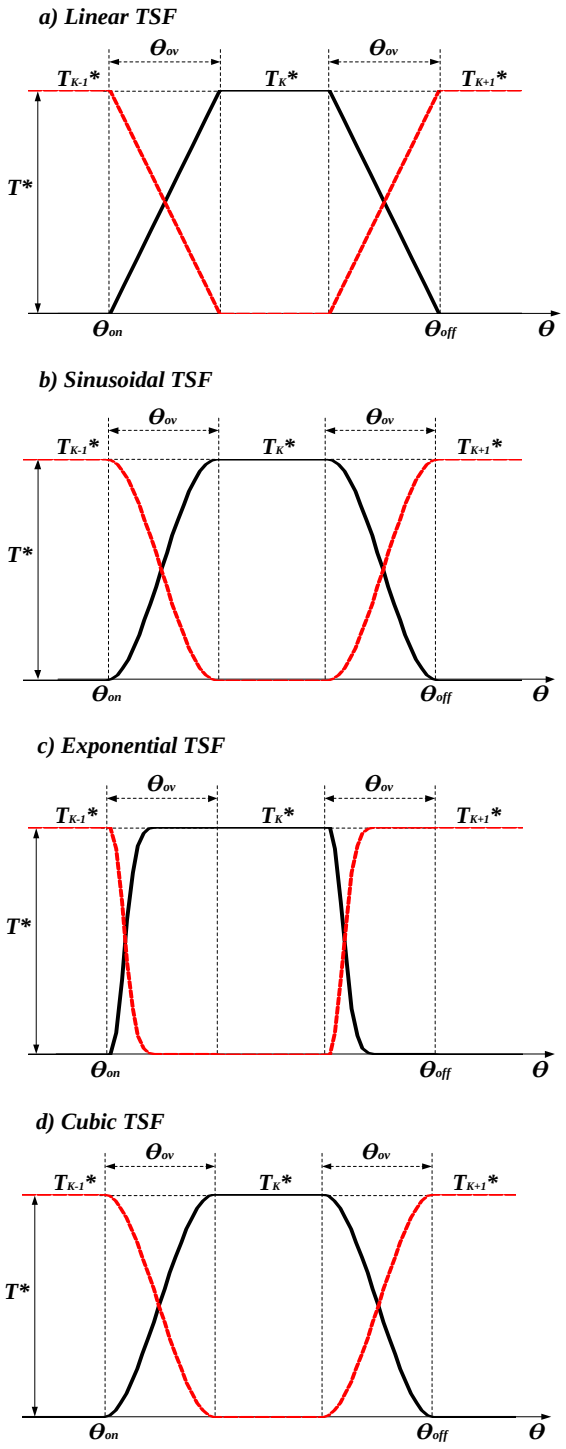

Fig. 5: Typical profiles of phase torque obtained with a) linear, b) sinusoidal, c) exponential and d) cubic TSFs

In the case of linear TSF, function f_{rise} is defined as,

$$f_{rise}(\theta) = \frac{\theta - \theta_{on}}{\theta_{ov}} \tag{2}$$

in case of sinusoidal TSF, as

$$f_{rise}(\theta) = \left[\sin\left(\frac{\pi}{2} \cdot \frac{\theta - \theta_{on}}{\theta_{ov}}\right)\right]^2 \tag{3}$$

in case of exponential TSF, as

$$f_{rise}(\theta) = 1 - \exp\left(\frac{-(\theta - \theta_{on})^2}{\theta_{ov}}\right) \tag{4}$$

in case of cubic TSF, as

$$f_{rise}(\theta) = \frac{3 \cdot (\theta - \theta_{on})^2}{{\theta_{ov}}^2} - \frac{2 \cdot (\theta - \theta_{on})^3}{{\theta_{ov}}^3} \tag{5}$$

For these four TSFs, function f_{fall} can be defined as follows:

$$f_{fall}(\theta) = 1 - f_{rise}(\theta + \theta_{ov} - \theta_{off} + \theta_{on}) \tag{6}$$

The number of the degrees of freedom (DOFs) for these four TSFs is 2.

B. Piecewise Cubic TSF

The piecewise cubic TSF is a generalization of the cubic one with an arbitrary number of DOFs [8]. Figure 6 shows the profile of the piecewise cubic TSF with 6 DOFs as an example. In this figure, it is transformed in a spatial-dependent model in which the piecewise cubic TSF is represented in terms of number of strokes, stroke angle θ_s is given by $\theta_s = 360^\circ/(N_{ph} \cdot N_r)$. One stroke is divided into some fractions with the number of DOFs. The linear variation between two consecutive points is interpolated using a cubic spline method (shown with red line in figure 6 in which the TSF is represented in terms of number of strokes). The number of DOFs varies between two and an arbitrary number (for the general approach).

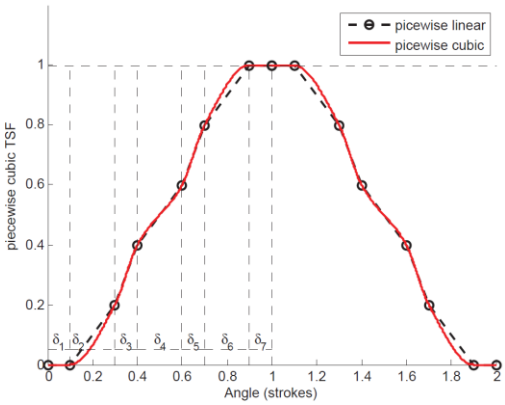

Fig. 6: Piecewise cubic TSF with 6 DOFs (δ_1, δ_2, δ_3, δ_4, δ_5 and δ_6) [8]

Lower copper losses can be obtained with more DOFs. However, it increases the complexity of the optimization problem and the computational time. By way of compromise, 5 is chosen as the number of DOFs [8].

V. CONVERTER LOSSES

To evaluate the performance of the control strategies, the asymmetric H-bridge converter in figure 7 has been chosen to drive the machine. It should be noted that in the simulation, only the classical soft-chopping strategy is adopted as it produces lower switching losses than the hard-chopping strategy [21].

Each H-bridge is assumed being composed of SEMIKRON modules, namely SEMiX151GAL12E4s and SEMiX151GAR12E4s as shown in figure 8. To compute the semiconductor losses in the converter, which consist of conduction and switching losses, as accurately as possible, the losses are calculated at every time step of simulation based on look-up tables created according to the manufacturer datasheets in figures. 9 and 10 [20]. For the conduction losses of the IGBTs and the freewheeling diodes (the anti-parallel diodes do not conduct the currents in this converter), which are the product of the current flowing through and the voltage drop across the devices, 1-D lookup tables of the voltage drop as function of the current are adopted. For the switching losses of the IGBTs, switching-detection blocks are used to detect the on and off switching instants, and subsequently 2-D lookup tables are used to determine turn-on and turn-off energy losses based on the corresponding current and blocking voltage at that switching instant. Since the characteristics of the switching energies are given only at 600-V blocking voltage in the datasheet, the linear interpolation is used to calculate the switching energies at other values of blocking voltage. The calculation of the switching losses of the diodes is carried out in the same way except that the turn-on energy losses are so small that they can be omitted [22]. Finally, the average losses are obtained by averaging those instantaneous loss values over the fundamental period (i.e. one stroke of the SRM operation, or 15° in case of an 8/6 SRM). It should be noted that the parameters of the semiconductors depend also on the junction temperature, so in this paper the parameters used are at 150°C. The calculation steps are summarized in figure. 11.

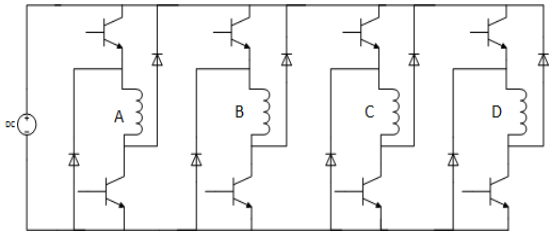

Fig. 7: Asymmetric H-Bridge converter for feeding all four phases (A, B, C and D) of the SRM independently. (Drawn to use in FP7 ITN Project 607361 ADEPT [23])

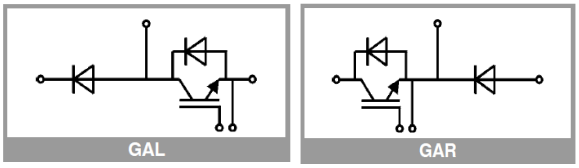

Fig. 8: Power semiconductor modules used to construct one phase leg. Left: SEMiX151GAL12E4, right: SEMiX151GAR12E4. (Drawn by the manufacturer, SEMIKRON)

TABLE II: ELECTRICAL CHARACTERISTICS OF SEMIX151GAL/GAR12E4

IGBTs	
Collector-to-emitter voltage	1200 V
Nominal collector current	150 A
Collector-to-emitter saturation voltage	2.05 V @ 150 A 25°C
Turn-on switching energy	16.6 mJ @ 150 A 600 V
Turn-off switching energy	18.4 mJ @ 150 A 600 V
Free-Wheeling Diodes	
Reverse biased voltage	1200 V
Nominal current	150 A
forward voltage drop	2.46 V @ 150 A 25°C
Turn-off switching energy	8.9 mJ @ 150 A 600 V

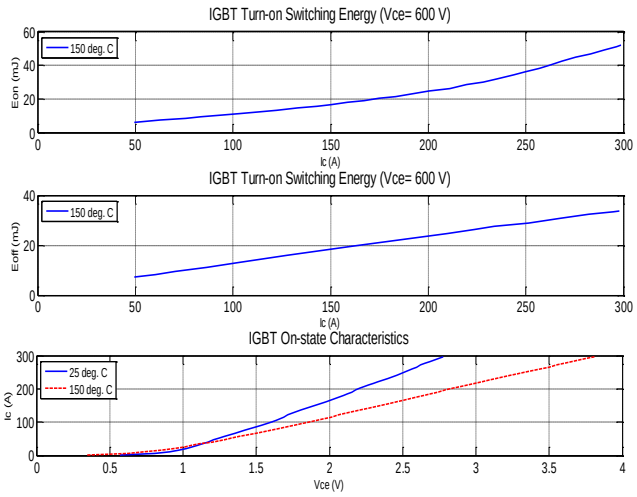

Fig. 9: Electrical loss characteristics of the IGBTs in SEMiX151GAL/GAR12E4. Top: turn-on energy dependence on the collector current, middle: turn-off energy dependence on the collector current, bottom: on-state characteristics

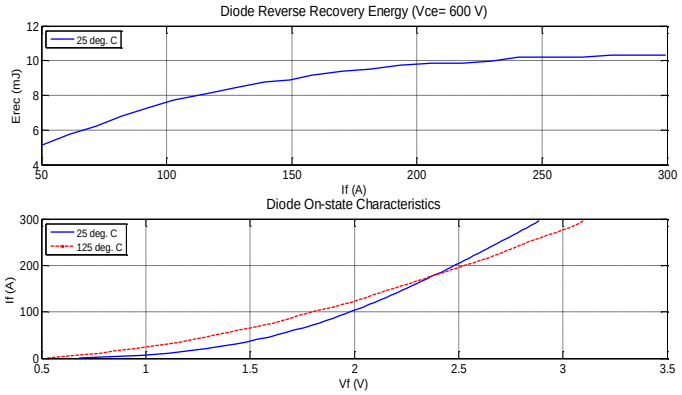

Fig. 10: Electrical loss characteristics of the freewheeling diodes in SEMiX151GAL/GAR12E4. Top: reverse recovery energy (turn-off energy) dependence on the collector current, bottom: on-state characteristics

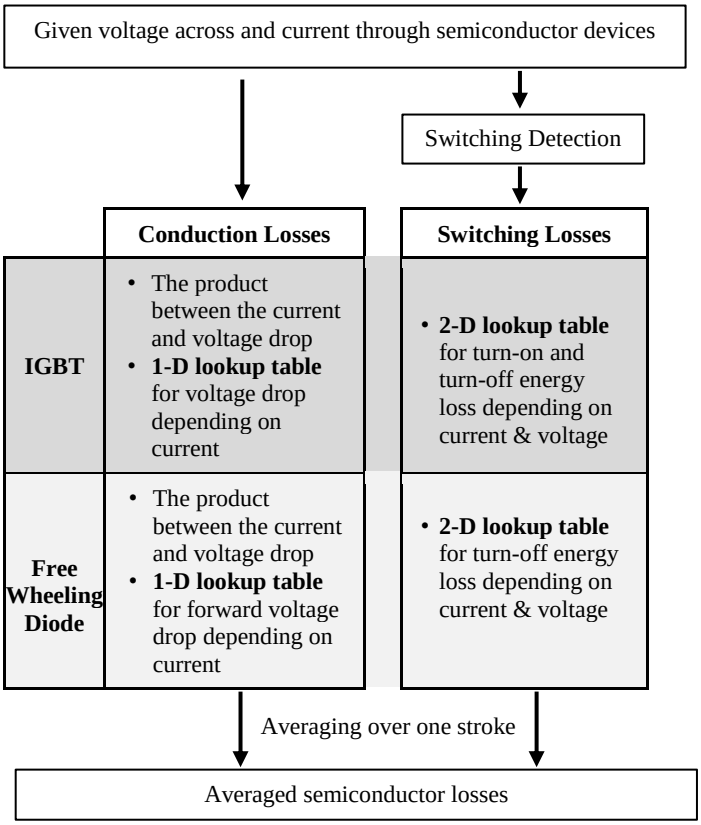

Fig. 11: Online semiconductor loss calculation steps

VI. Simulation Results

The simulation is conducted in MATLAB/Simulink for both the converter part and the machine part, in which a look-up table of flux linkage from finite element analysis in section II is integrated. The 307-V dc-bus is used for the converter to feed the machine.

A. *Torque Ripple Reduction*

In figures 12 and 13, the simulation results using firing angle control and piecewise cubic TSF are compared under the condition of 200 rpm, 45 Nm and 1000 rpm, 95 Nm respectively. It can be seen that the peak-to-peak torque ripple is 29.82 Nm in figure 12 (a), 6.95 Nm in figure 12 (b), 50.67 Nm in figure 13 (a) and 7.04 Nm in figure 13 (b). It can be seen that with the piecewise cubic TSF the peak-to-peak torque ripple is much smaller than with the firing angle control.

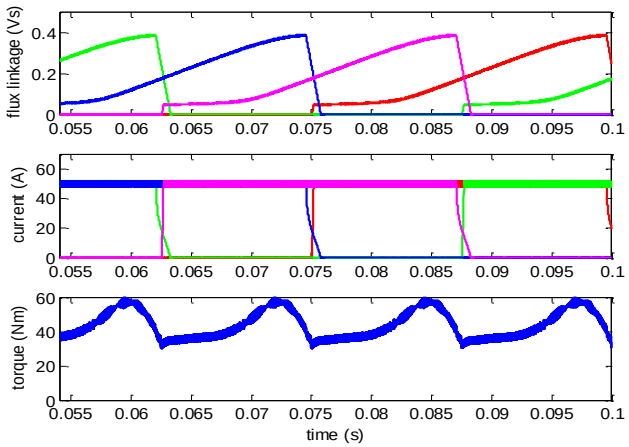

(a) Firing angle control

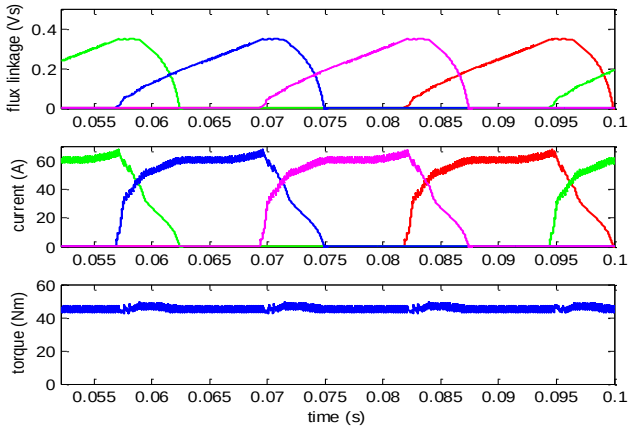

(b) Piecewise cubic TSF

Fig. 12: Simulation results at 200rpm speed and 45Nm reference torque. (a) Firing angle control (b) Piecewise cubic TSF

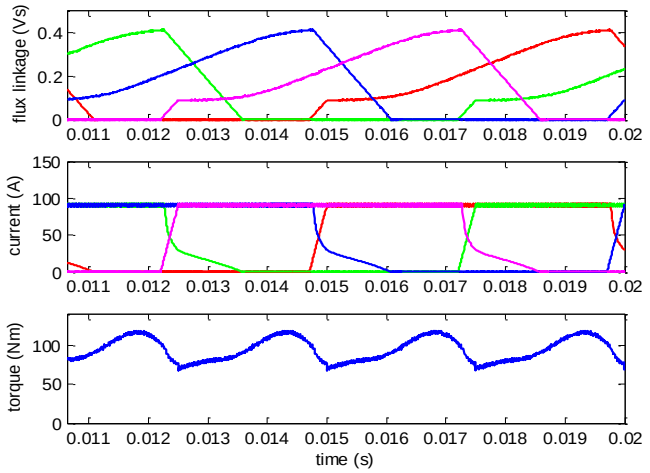

(a) Firing angle control

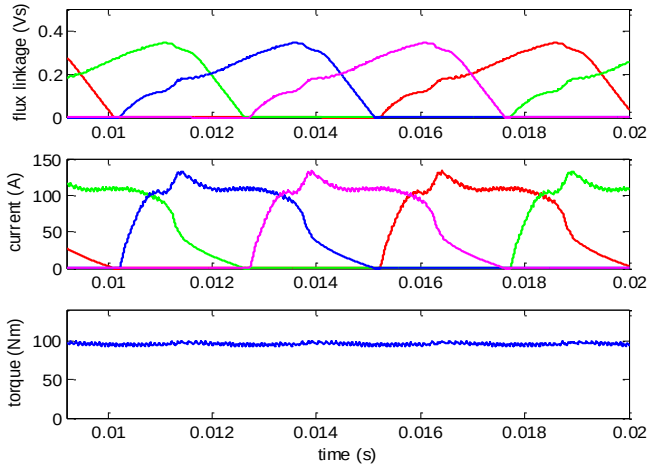

(b) Piecewise cubic TSF

Fig. 13: Simulation results at 1000rpm speed and 95Nm reference torque. (a) Firing angle control (b) Piecewise cubic TSF

Figure 14 shows the relative peak-to-peak torque ripple dependence on reference torque (from 10 Nm to 175 Nm, in steps of 10 Nm) and speed (from 100 rpm to 1000 rpm, in steps of 100 rpm). It can be seen that the relative peak-to-peak torque ripple decreases by more than half when the piecewise cubic TSF control is used.

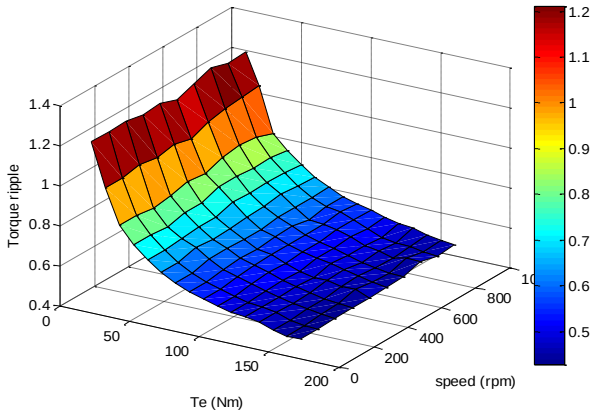

(a) Firing angle control

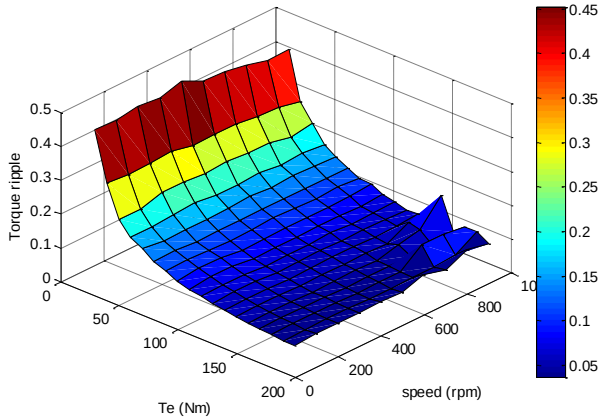

(b) Piecewise cubic TSF

Fig. 14: Relative peak-to-peak torque ripple dependence on reference torque and speed. (a) Firing angle control (b) Piecewise cubic TSF

B. Copper Losses Reduction

Copper losses in the SRM for these two control strategies as function of speed and average torque are obtained. Simulations have been carried out at different speeds from 100 rpm to 1000 rpm varying the torque between 10 Nm and 150 Nm. Figure 15 shows the copper losses surfaces dependence on reference torque and speed for firing angle control and piecewise cubic TSF. The copper losses are reduced when the piecewise cubic TSF is used.

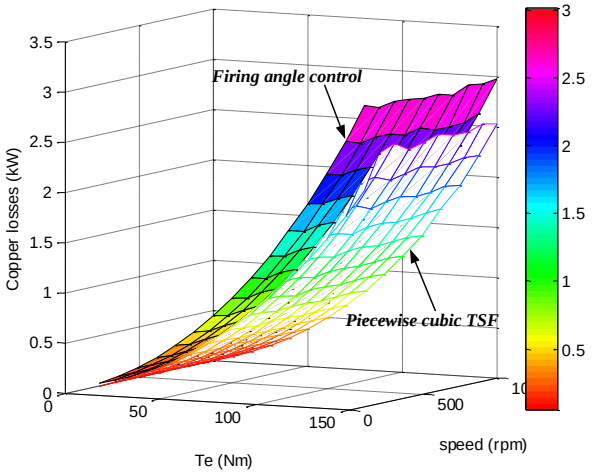

Fig. 15: Copper losses in the SRM as function of torque and speed for firing angle control and piecewise cubic TSF

C. *Conduction Losses, Switching Losses and Converter Losses*

Figures 16, 17 and 18 show conduction losses, switching losses and total converter losses, respectively, for aforementioned control strategies as function of speed at 150 Nm and rated torque 90 Nm. Simulations have been carried out at different speeds from 100 rpm to 1000 rpm. It can be seen that conduction, switching and total losses with the piecewise cubic TSF are lower than those with FA control at all considered speeds and torques. The total converter losses are reduced by 10% to 30% in the considered torque and speed ranges when the piecewise cubic TSF is used.

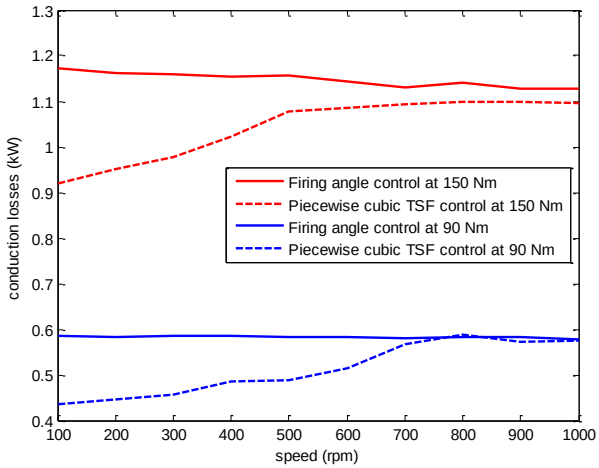

Fig. 16: Conduction losses in the converter for FA control and piecewise cubic TSF control at 150 Nm and 90 Nm

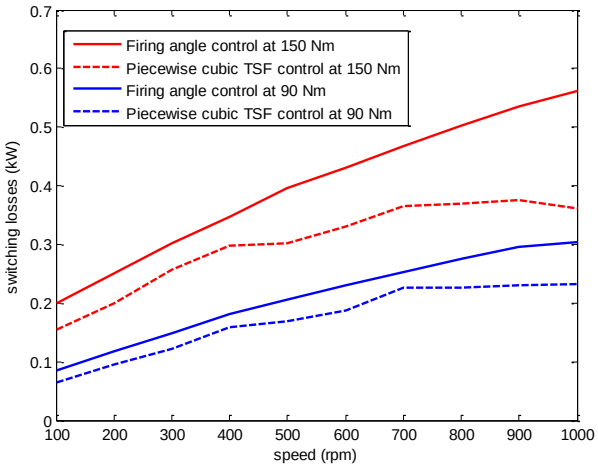

Fig. 17: Switching losses in the converter for FA control and piecewise cubic TSF control at 150 Nm and 90 Nm

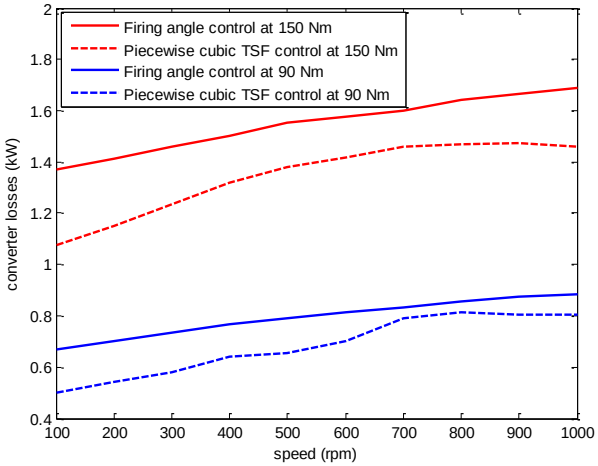

Fig. 18: Converter losses for FA control and piecewise cubic TSF control at 150 Nm and 90 Nm

D. *Total Efficiency of The SRM Drive System*

Figure 19 shows the efficiency of the SRM and its converter dependence on speed for both control strategies at 90 Nm which is the rated torque. It can be seen that the total efficiency of the SRD with the piecewise cubic TSF is much higher than that with firing angle control at different speeds. On the other hand, in figure 20, the total efficiency with the piecewise cubic TSF is still higher at different torques with a constant speed at 1000 rpm. The efficiency seems to be over realistic, because iron losses and mechanical losses in the SRM have not been considered in this paper.

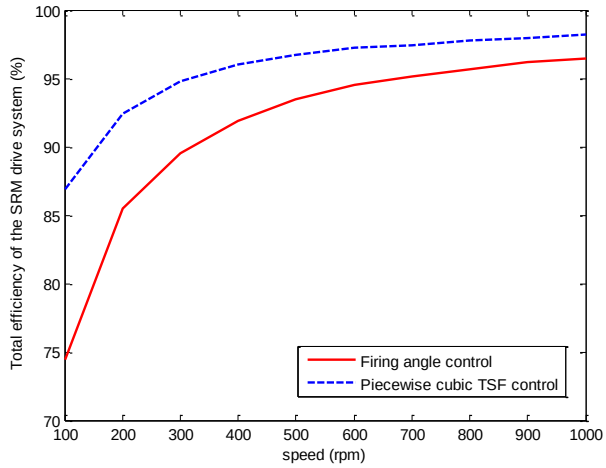

Fig. 19: Total efficiency of the SRD for FA control and piecewise cubic TSF control at 90 Nm

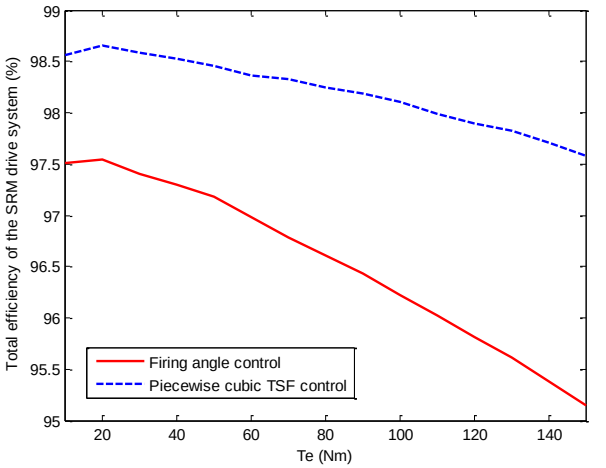

Fig. 20: Total efficiency of the SRD for FA control and piecewise cubic TSF control at 1000 rpm

VII. Conclusion

In this paper firing angle control and piecewise cubic TSF control strategies have been compared in terms of torque ripple reduction as well as copper and converter losses reduction. The flux linkage characteristics of the SRM, necessary for the modeling, have been obtained by Gmsh and GetDP. The simple SRM model has been used to identify the parameters of these control strategies as function of speed and torque in order to provide the copper losses minimization. The MATLAB function fminsearchbnd has been used to get the turn on and turn off angles look-up tables for the firing angle control and the five parameters for the piecewise cubic TSF control. The simulation results demonstrate the potential possibility of the reduction of the torque ripple by more than 50% using the piecewise cubic TSF compared to the firing angle control strategy, at the same time, the copper losses are reduced by 20% approximately in the considered torque and speed ranges. The conduction losses in the converter are reduced when using the piecewise cubic TSF especially at very low speeds (lower than 700 rpm), at the same time, the switching losses with piecewise cubic TSF are even lower when the speed is higher, and consequently the total converter losses are reduced by 10% to 30%. The total efficiency of the SRM drive system with the piecewise cubic TSF is much higher than that with firing angle control at different speeds and torques.

As future work the implementation of variable hysteresis bandwidth for firing angle control and piecewise cubic TSF control can be considered, for instance, the bandwidth for the hysteresis current control can be used as 10% of the reference current value. Moreover, the performances of the SRD with both control strategies can be assessed considering different driving cycles.

Acknowledgment

This paper is part of the ADvanced Electric Powertrain Technology (ADEPT) project which is an EU funded Marie Curie ITN project, grant number 607361. Within ADEPT a virtual and hardware tool are created to assist the design and analysis of future electric propulsions. Especially within the context of the paradigm shift from fuel powered combustion engines to alternative energy sources (e.g. fuel cells, solar cells, and batteries) in vehicles like motorbikes, cars, trucks, boats, planes. The design of these high performance, low cost and clean propulsion systems has stipulated an international cooperation of multiple disciplines such as physics, mathematics, electrical engineering, mechanical engineering and specialisms like control engineering and safety. By cooperation of these disciplines in a structured way, the ADEPT program provides a virtual research lab community from labs of European universities and industries [23].

The authors would like to thank the European Union for the funding of this research (FP7 ITN Project 607361 ADEPT and FP7 IAPP Project 324345 DeMoTest-EV).

References

[1] K. M. Rahman, B. Fahimi, G. Suresh, A. V. Rajarathnam, M. Ehsani, *Advantages of Switched Reluctance Motor Applications to EV and HEV: Design and Control Issues*, IEEE Transactions on Industry Applications, Vol. 36, No. 1, pp. 111-121, 2000.

[2] V. P. Vujicic, *Minimization of Torque Ripple and Copper Losses in Switched Reluctance Drive*, IEEE Transactions on Power Electronics, Vol. 27, No. 1, 2012.

[3] H. Ishikawa, M. Uraji, H. Naitoh, *A New Current Control for Eddy Current Loss Reduction of Switched Reluctance Motors*, Control and Modeling for Power Electronics (COMPEL), 2013.

[4] D. Schramm, B. Williams, T. Green, *Torque Ripple Reduction of Switched Reluctance Motors by Phase Current Optimal Profiling*, Power Electronics Specialists Conference, PESC '92 Record., 23rd Annual IEEE, Vol.2, pp. 857 -860, 1992.

[5] M. Ilic-Spong, T. J. E. Miller, S. R. Macminn, J. S. Thorp, *Instantaneous Torque Control of Electric Motor Drives*, Power Electronics, IEEE Transactions, Vol. PE-2, pp. 55 -61, 1987.

[6] L Husain, M. Ehsani, *Torque Ripple Minimization in Switched Reluctance Motor Drives by PWM Current Control*, Power Electronics, IEEE Transactions, Vol. 11, pp. 83 -88, 1996.

[7] S. Sahoo, S. Panda, J. X. Xu, *Indirect Torque Control of Switched Reluctance Motors Using Iterative Learning Control*, Power Electronics, IEEE Transactions, Vol. 20, pp. 200 - 208, 2005.

[8] A. Pop, V. Petrus, C. S. Martis, V. Iancu, J. Gyselinck, *Comparative Study of Different Torque Sharing Functions for Losses Minimization in Switched Reluctance Motors Used in Electric Vehicles Propulsion*, Optimization of Electrical and Electronic Equipment (OPTIM), 2012.

[9] X. Xue, K. Cheng, S. Ho, *Optimization and Evaluation of Torque-Sharing Functions for Torque Ripple Minimization in Switched Reluctance Motor Drives*, Power Electronics, IEEE Transactions, Vol. 24, pp. 2076 -2090, 2009.

[10] X. Xue, K. Cheng, N. Cheung, *Evaluation of Torque Sharing Functions for Torque Ripple Minimization of Switched Reluctance Motor Drives in Electric Vehicles*, Power Engineering Conference, pp. 1 -6, 2008.

[11] Ye. Jin, Emadi. Ali, *Power Electronic Converters for 12/8 Switched Reluctance Motor Drives: A comparative analysis*, Transportation Electrification Conference and Expo (ITEC), IEEE, vol., no., pp.1,6, 2014

[12] K. Ha, C. Lee, J. Kim, K, R., S. Oh, *Design and Development of Low-Cost and High-Efficiency Variable-Speed Drive System With Switched Reluctance Motor*, Industry Applications, IEEE Transactions, Vol.43, no.3, pp.703-713, May-June, 2007.

[13] H. Lovatt, *Power Converter Rating for Switched Reluctance Motors*, Energy Conversion Congress and Exposition (ECCE), 2014 IEEE, pp. 1356-1359, 14-18 Sept. 2014.

[14] M. Barnes, C. Pollock, *Power Electronic Converters for Switched Reluctance Drives*, Power Electronics, IEEE Transactions, Vol. 13, pp. 1100-1111, 1998.

[15] Gmsh: a three-dimensional finite element mesh generator with built-in pre- and post-processing facilities, http://geuz.org/gmsh/

[16] GetDP: a General Environment for the Treatment of Discrete Problems, http://geuz.org/getdp/

[17] Open Numerical Engineering LABoratory, http://onelab.info/wiki/

[18] Electric Machines, http://onelab.info/wiki/Electric_Machines

[19] T. Miller, *SPEED's Electric Motors*, University of Glasgow, 2002-2004.

[20] S. Munk-Nielsen, L. Tutelea, U. Jaeger, *Simulation with Ideal Switch Models Combined with Measured Loss Data Provides a Good Estimate of Power Loss*, Industry Applications Conference, IEEE, vol.5, pp.2915-2922, 2000.

[21] T.J.E. Miller, *Switched Reluctance Motors and their Control*, Magna Physics &Oxford. 1993.

[22] P. Haaf, and J. Harper, *Understanding Diode Reverse Recovery and Its Effect on Switching Losses*, Fairchild Power Seminar, 2007.

[23] A. Stefanskyi, A. Dziechciarz, F. Chauvicourt, G. E. Sfakianakis, K. Ramakrishnan, K. Niyomsatian, M. Curti, N. Djukic, P. Romanazzi, S. Ayat, S. Wiedemann, W. Peng, S. Sjipetic, *Researchers within the EU funded Marie Curie ITN project ADEPT, grant number 607361*, 2013-2017.